Effects of Loading Rate on Fracture Behavior of Low-Alloy Steel with Different Grain Sizes

G.Z. WANG, X.C. REN, and J.H. CHEN

Four-point bend (4PB) tests of notched specimens loaded at various loading rates, for low alloy steel with different grain sizes, were done, and the microscopic observation and finite-element method (FEM) calculations were carried out. It was found that for the coarse-grained (CG) microstructure, an appreciable drop in notch toughness with a loading rate of around 60 mm/min appeared, and further increasing the loading rate leads to a slight additional decrease in notch toughness. For the fine-grained (FG) microstructure, the effect of loading rate was not apparent. The change in toughness resulted from a change of the critical event controlling the cleavage fracture with increasing loading rate. For the CG microstructure with a lower cleavage-fracture stress (σ_f), with an increasing loading rate, the critical event of cleavage fracture can be changed from the propagation of a pearlite colony–sized crack or a ferrite grain–sized crack, through the mixed critical events of crack propagation and crack nucleation, then to crack nucleation. This change deteriorates the toughness. For the FG microstructure with a higher cleavage-fracture stress, the critical event of cleavage fracture is the crack propagation and does not change in the loading-rate range from 120 to 500 mm/min. The measured σ_f values do not change with loading rate, as long as the critical event of cleavage fracture does not change. The higher notch toughness of the FG microstructure arises from its higher σ_f and the critical plastic strain (ε_{pc}) for initiating a crack nucleus, and the fracture behavior of this FG steel is not sensitive to loading rate in the range of this work.

I. INTRODUCTION

IT is well known that changes in loading rate and test temperature influence the deformation (yield and flow) and fracture behavior of steel. The most significant effect of increasing loading rate is to shift the quasi-static K_{Ic} transition curve toward higher temperatures, that is, to raise the temperatures at which cleavage may occur.[1] This is very critical for structural steel components. The high-strain-rate sensitivity of these steels makes the safety design on the basis of quasi-static behavior rather poor. Therefore, the reliability of structures possibly loaded at higher loading rates requires the knowledge of the corresponding material fracture behavior.

Couque *et al.*[2] investigated the fracture behavior of a plain-carbon steel with various microstructures at two loading rates corresponding to quasi-static and high-rate loading (Charpy impact test) and over a range of temperatures. The effects of temperature, loading rate, and various microstructural parameters on the initiation of plane-strain fracture were explored. Zurek *et al.*[3] studied the influence of dynamic spall loading on the cleavage-fracture behavior of a mild-carbon steel. Lee *et al.*[4] characterized fracture toughness under both dynamic and quasi-static loading over a wide range of temperatures and investigated the effects of microstructure on the fracture toughness of an HY-100 steel. In a recent work,[5] the brittle fracture initiation and crack propagation of the heat-affected zone (HAZ) of a structural steel under static and dynamic loading were examined. In some other recent works,[6–9] the effects of loading rate on the ductile-fracture behavior of various steels were explored.

However, the effects of loading rate on the brittle-fracture mechanism, fracture stress, and toughness of various steels have not been understood completely. Specifically, the correlations of microstructure with notch toughness at different loading rates remain to be learned. In engineering structures and components possibly loaded at a higher loading rate, notches may be difficult to avoid, and some notchlike geometries are necessary for structure design. Therefore, the understanding of notch toughness at higher loading rates is also very important.

This work focuses on the effect of loading rate on the notch toughness of low-alloy steels with different grain sizes at the same test temperature. Combining microscopic observation, finite-element method (FEM) calculations, measurements of the cleavage-fracture stress (σ_f), and the new cleavage-fracture model[10,11,12] for a notched specimen, the mechanism of the effect of loading rate on the notch toughness of the steels is analyzed from the viewpoint of change of the critical event for cleavage fracture.

II. EXPERIMENTAL

A. *Materials and Specimens*

A low-alloy steel, of the composition shown in Table I, was used. This steel was a clean steel with low contents of inclusions and impurity elements. Two types of heat treatments were carried out on the steel for obtaining the desired microstructures and grain sizes. One was to heat the steel

G.Z. WANG and J.H. CHEN, Professors, are with State Key Laboratory of New Nonferrous Metal Materials, Lanzhou University of Technology (Gansu University of Technology), Lanzhou, Gansu, 730050, Peoples Republic of China. Contact e-mail: wanggz@lut.cn X.C. REN, Doctorate Student, is with the College of Material Science and Engineering, Beijing University of Science and Technology, Beijing 100081, People's Republic of China.

Manuscript submitted March 6, 2003.

Table I. Compositions of Used Steel (Weight Percent)

C	Mn	Si	Mo	Cr	V	S	P	B
0.06	1.36	0.23	0.21	0.19	0.03	0.009	0.020	0.0017

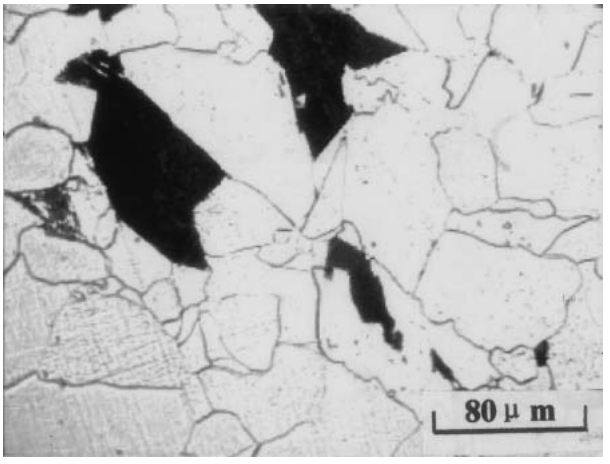

(*a*)

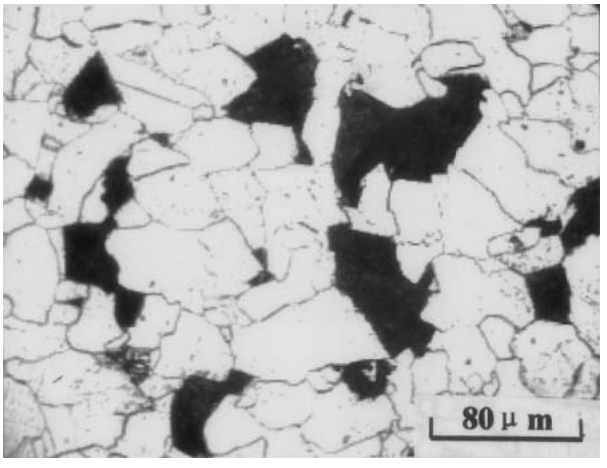

(*b*)

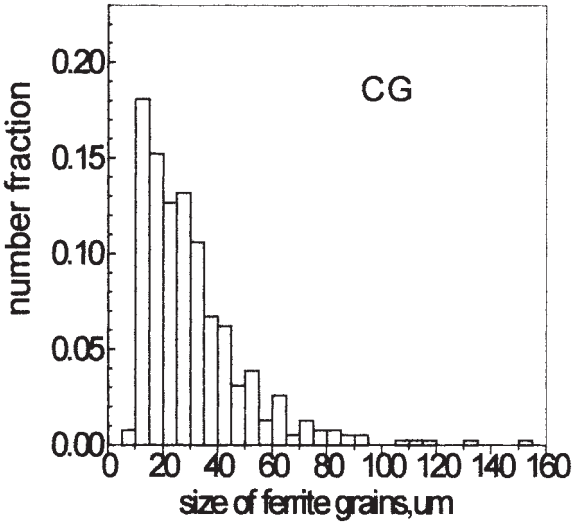

(*a*)

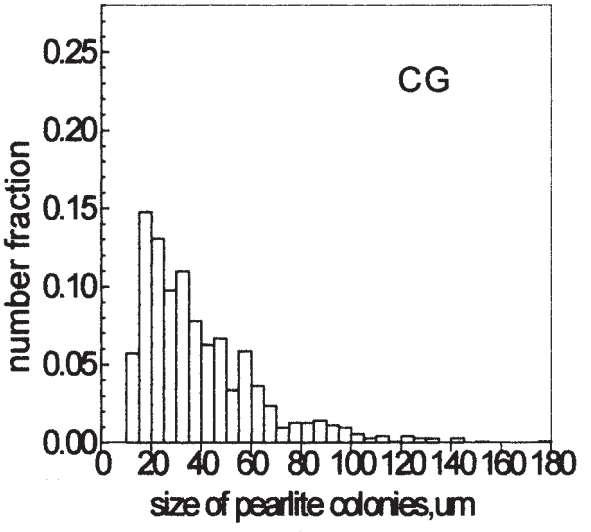

(*b*)

Fig. 2—Histograms of size distributions of (*a*) ferrite grains and (*b*) pearlite colonies of CG microstructure.

to 1000 °C for 6 hours, followed by a furnace cool. The microstructure, designated as the coarse-grained (CG) one, contains ferrite grains with about 7 pct pearlite colonies and a few carbide particles, as shown in Figure 1(a). The fraction of pearlite colonies was estimated by the area fraction of pearlite colonies on ten scanning electron microscope (SEM) photographs. Histograms of the size distributions of ferrite grains and pearlite colonies are shown in Figure 2, and the grain sizes are as large as those in the CG region in the HAZ of the weldment.[13,36] For comparison, the second heat treatment consisted of 945 °C/45 minutes, followed by a furnace cool. The grain sizes are finer and the microstructure is designated as the fine-grained (FG) one (Figure 1(b)). Related histograms are shown in Figure 3.

Eight-millimeter-diameter round bars with a 50-mm gage length were used for the tensile tests. Four-point bend (4PB) specimens were cut in the longitudinal-transverse orientation. The dimensions and loading method (indicated by arrows) of single- and double-notched specimens are shown in Figure 4. The double-notched specimens are used for observing the remaining microcracks.

B. *Mechanical Tests*

Tensile specimens were tested at various loading rates at a temperature of −100 °C. The variations of the yield strength (σ_y), work-hardening exponent (n), and coefficient K in the power-hardening relation $\sigma = K\sigma^n$ with loading rate (strain rate) were measured. The 4PB tests were carried out at different loading rates of 1, 30, 60, 120, 240, 360, and 500 mm/min by SHIMADZU AG-10T universal test machine at −100 °C, and the curves of the load and load-line displacement were recorded automatically. The quotient obtained by dividing the load-line displacement at fracture by the loading rate was the total test time for each loading rate. The fracture load (P_f) and the absorbed energy (W) for fracture

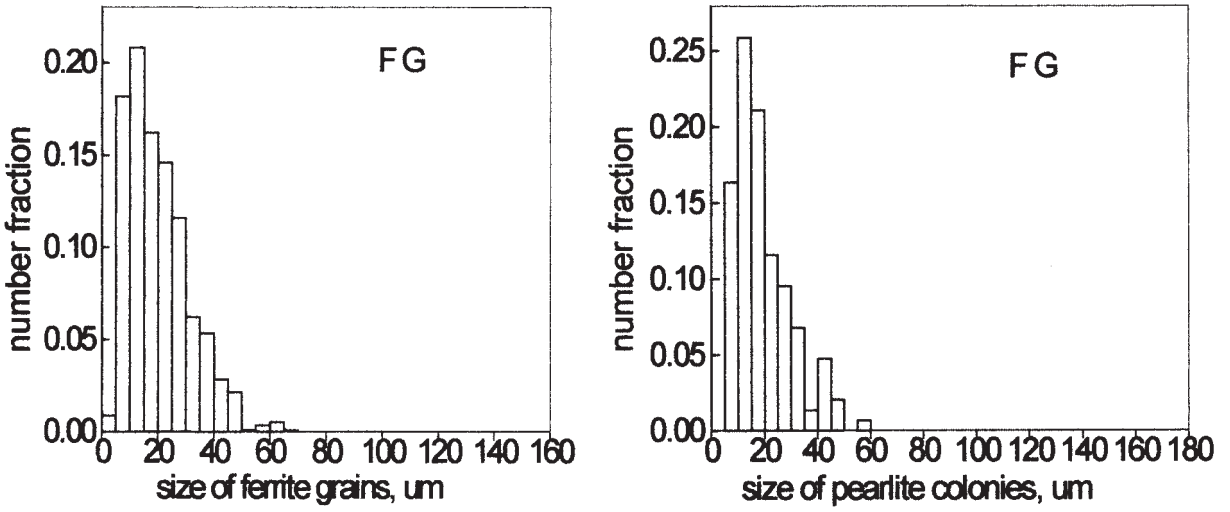

Fig. 3—Histograms of size distributions of (*a*) ferrite grains and (*b*) pearlite colonies of FG microstructure.

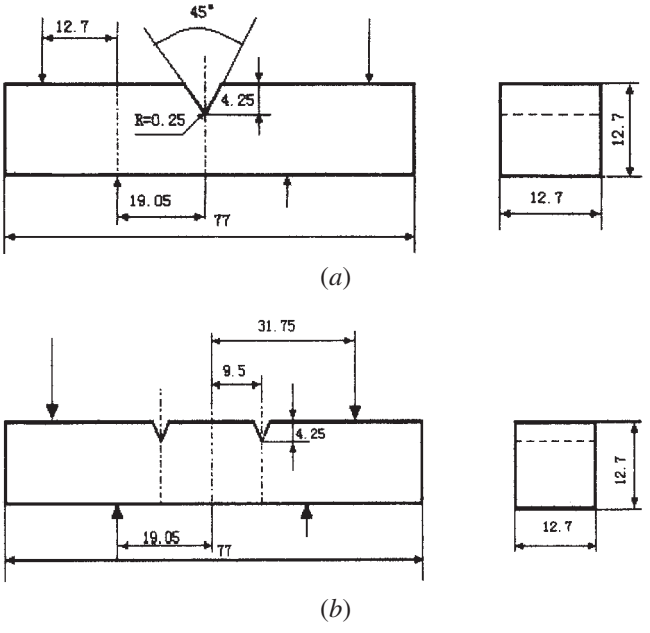

Fig. 4—Dimensions (in millimeters) of 4PB test specimens with (*a*) single notch and (*b*) double notches.

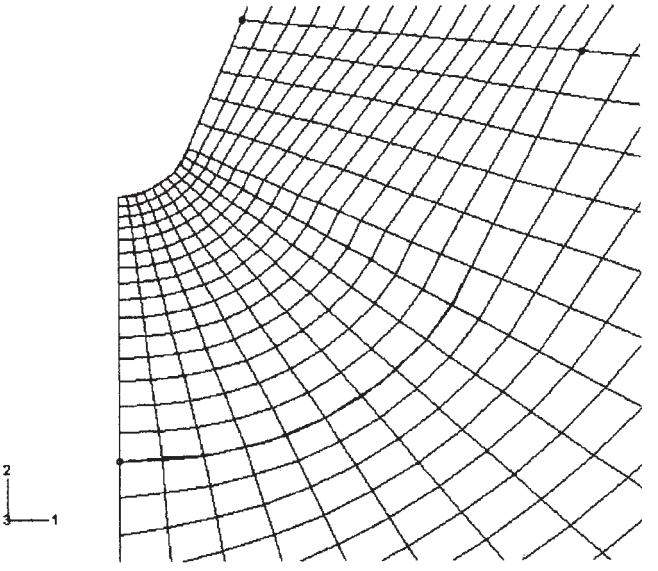

Fig. 5—The element arrangement in the vicinity of the notch root in the FEM model.

(the area covered by the load-displacement curve) were measured by the load-displacement curve.

C. *Microscopic Observation*

Fracture surfaces of all specimens were observed in detail with an Hitachi S-520 SEM. The initiation sites of cleavage fracture were located by tracing the river-pattern strips back to their origins. The distance of the cleavage-initiation site from the tip of the blunted notch was measured as X_f. For specimens with fibrous cracking prior to cleavage, the length of the fibrous crack was measured. For double-notched specimens, fracture occurred at one notch and the critical condition was reached in the vicinity of the surviving notch. The metallographic sections perpendicular to the surviving notch root were made to observe the remaining crack and identify the critical event of cleavage.

D. *Finite-Element Method Calculation*

The maximum normal stress (σ_{yy}) on the plane directly ahead of the notches and the effective plastic strain (ε_p) ahead of the notches were calculated at applied loads, from the elastic regime to over general yield for the single-notched 4PB specimens tested at various loading rates at −100 °C. A two-dimensional model with four-node biquadratic plane-strain reduced-integration elements (CPE4R) was used with the ABAQUS/Explict code. Due to symmetry, only one-half of the geometry needs to be analyzed, and the numbers of elements and nodes are 3274 and 3420, respectively. The element arrangement in the vicinity of the notch root is shown in Figure 5. The minimum element

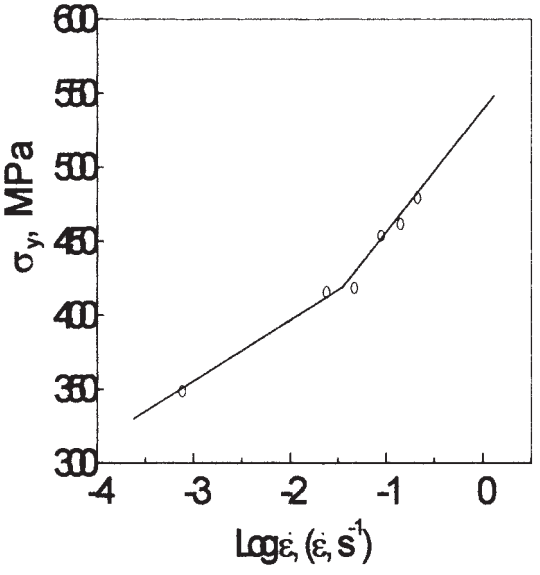

(*a*)

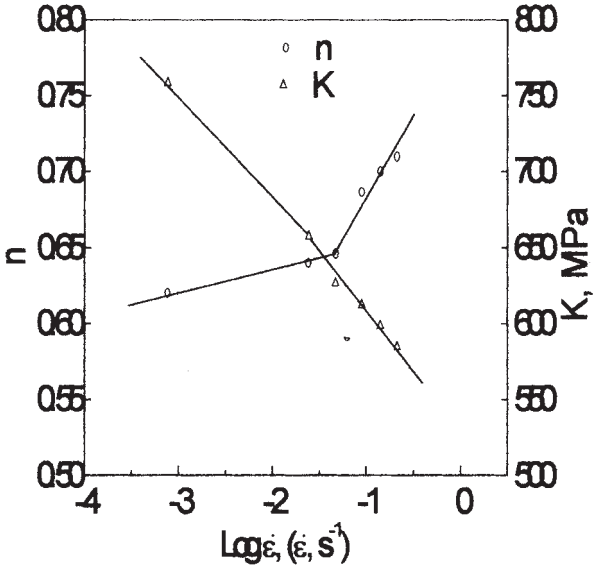

(*b*)

Fig. 6—The variations of (*a*) yield stress σ_y and (*b*) working-hardening exponent n and coefficient K with logarithm of strain rate $\dot{\varepsilon}$ for CG microstructure.

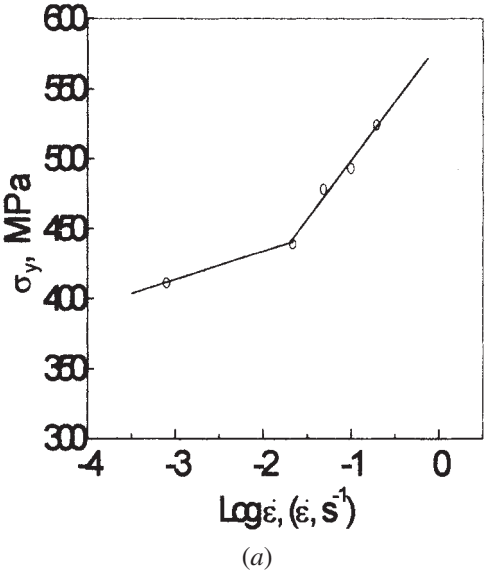

(*a*)

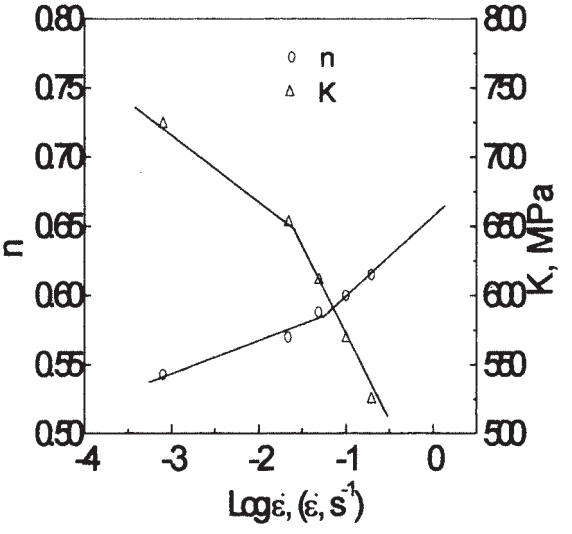

(*b*)

Fig. 7—The variations of (*a*) yield stress σ_y and (*b*) hardening exponent n and coefficient K with logarithm of strain rate $\dot{\varepsilon}$ for FG microstructure.

size is 25 μm at the notch tip. The stress-strain response of the material at different loading rates (measured by the tensile test) obeys the power-hardening relation $\sigma = K\varepsilon^n$. The yield strength, work-hardening exponent, and coefficient at different loading rates (strain rate) are obtained from the tensile-test results (Figures 6 and 7). The stress-strain curves at various strain rates were digitized and fit into the data for the input file of the FEM code. The various strain rates from the tensile tests were automatically used in different locations ahead of the notch by the FEM code in the FEM simulations. The value of P_{gy} was calculated by the applied load at which a plastic "hinge" spreads across the notched cross section to leave an elastic enclave located on the symmetry axis.[14]

E. *Measurement of Critical Values of Mechanical Parameters*

At a measured fracture load, the corresponding curves of tensile stress and effective plastic strain can be selected from the FEM calculation results. With the measured X_f value (the distance of the cleavage-initiation site from the tip of the blunted notch) as the abscissa, the corresponding ordinate value of the curve of strain distribution (Figure 9(b)) was taken as the critical plastic strain (ε_{pc}) for nucleating a crack. The corresponding ordinate value of the tensile stress of the stress-distribution curve (Figure 9(a)) was taken as the local cleavage-fracture stress.

III. RESULTS

A. *Results of Tensile Tests*

The tensile properties of the two CG and FG microstructures as functions of logarithm of strain rate ($\dot{\varepsilon}$) are shown

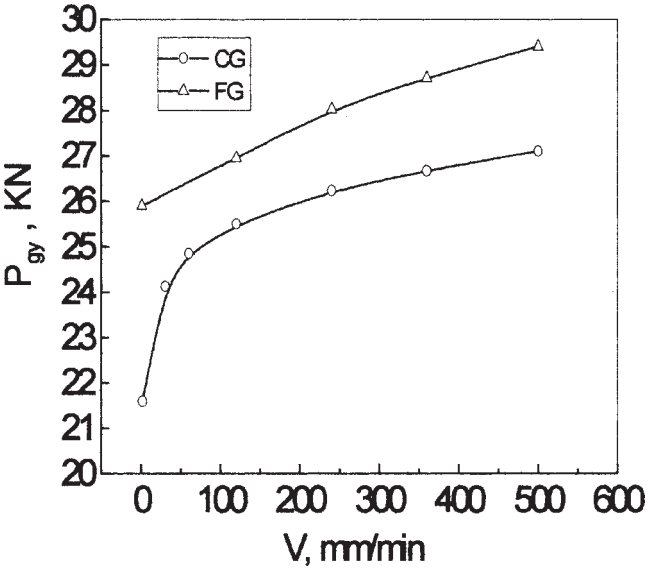

Fig. 8—The general yield load P_{gy} calculated by FEM as a function of loading rate V for the CG and FG microstructures.

in Figures 6 and 7, respectively. It can be seen from Figures 6 and 7 that the yield stress and work-hardening exponent increase linearly with the logarithm of strain rate ($\log\dot{\varepsilon}$) in two linear slopes. This result is similar to the works of References 15 and 16. Figures 6 and 7 also show that the σ_y value of the FG microstructure is larger than that of the CG one, but its n value is lower.

B. *The FEM Calculation Results of Stress and Strain Distributions for the 4PB Specimens*

The general yield load (P_{gy}) calculated by the FEM as a function of loading rate (V) is shown in Figure 8 for the two microstructures. The P_{gy} value increases with the loading rate, and the P_{gy} value of the FG microstructure is larger than that of the CG one. This change of P_{gy} with loading rate is caused by the change of the tensile properties of the materials with loading rate (Figures 6 and 7).

Typical results of the finite-element calculations of the maximum normal stress on the plane directly ahead of the notch and effective plastic-strain distributions ahead of the notch for the FG specimen with a loading rate of 240 mm/min are shown in Figure 9, where P is the applied load, and X is the distance to the notch root. In this figure, with increasing load ratio (P/P_{gy}), the normal stress and strain increase, and the peak σ_{yy} value moves away from the notch root, resulting in the extension of the areas under high σ_{yy} and ε_p values. This result is similar to the Griffith–Owen's result.[17] Figure 10 shows the variation of the peak stress σ_{yymax} and its location (X_{max}) ahead of notches with an applied-load ratio of P/P_{gy} for the specimens of the FG microstructure with various loading rates. The σ_{yymax} and X_{max} values increase with increasing P/P_{gy}. Before general yield ($P/P_{gy} < 1$), σ_{yymax} increases rapidly with P/P_{gy}, and, after that ($P/P_{gy} > 1$), it increases slowly. With increasing loading rate, σ_{yymax} increases, but X_{max} does not change significantly. The FEM calculation results of the stress and strain distribution for the specimens with various loading rates for the CG microstructure are similar to these, and the only difference is that the σ_{yy} value ahead of the notches of the CG specimens is lower than that of the FG one.

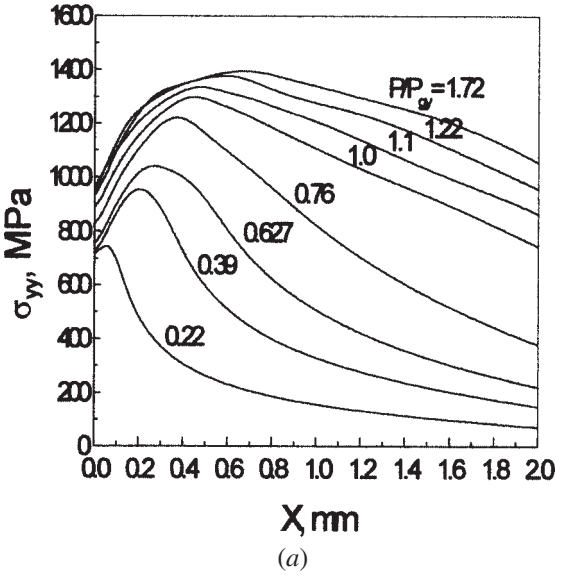

(*a*)

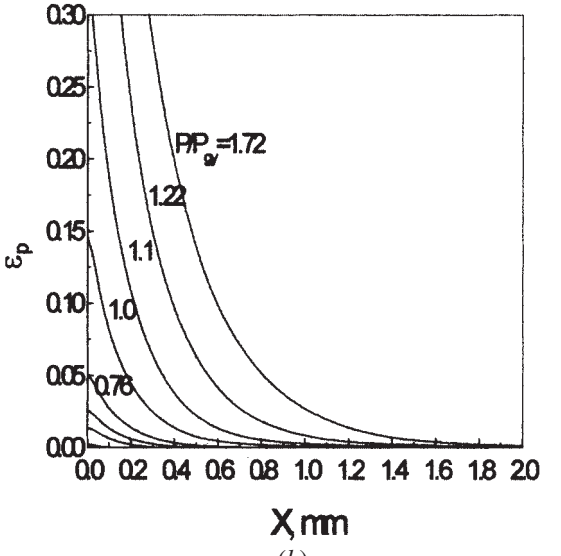

(*b*)

Fig. 9—Distributions of the (*a*) maximum normal stress σ_{yy} and (*b*) effective plastic strain ε_p in front of a notch calculated by FEM for the specimen of FG with a loading rate of 240 mm/min.

C. *Results of 4PB Tests*

1. *Results of mechanical tests*

The parameters measured from 4PB tests for the specimens with various loading rates for the CG and FG microstructures are shown in Tables II and III, respectively. Figures 11 and 12 summarize the variations of notch toughness (characterized by the ratio of the fracture load to the general yield load, P_f/P_{gy}, and the absorbed energy for fracture, W) against the loading rate for the CG and FG steels, respectively. For the CG microstructure, an appreciable drop in notch toughness of specimens with a loading rate of around 60 mm/min

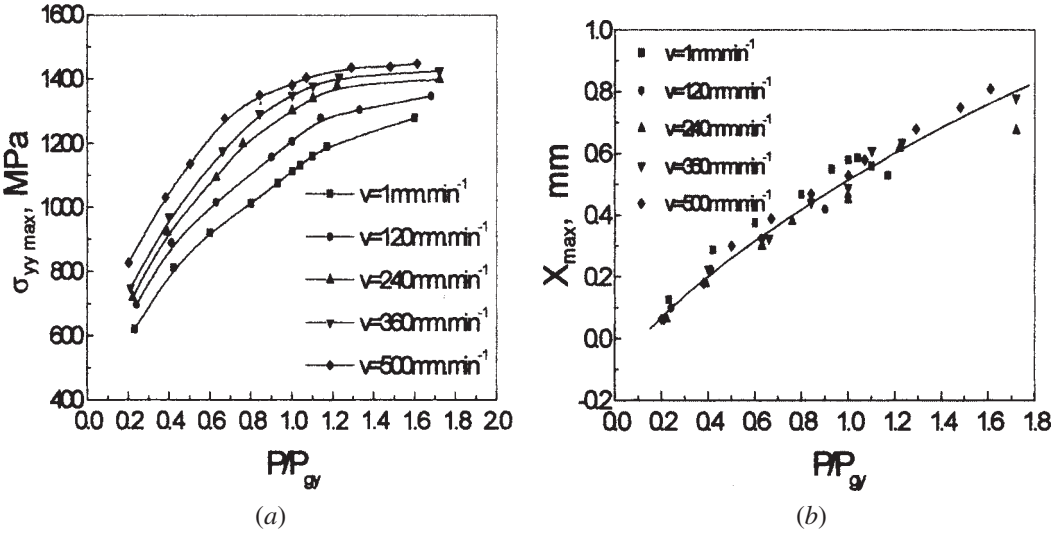

Fig. 10—The variation of the (*a*) peak stress σ_{yymax} and (*b*) its location X_{max} ahead of notches with applied load ratio P/P_{gy} for the specimens of FG with various loading rates.

Table II. The Parameters Measured from 4PB Tests for the Specimens with Various Loading Rates for CG

Number	V (mm/min)	P_f (KN)	P_f/P_{gy}	W (J)	X_f (μm)	σ_f (Mpa)	ε_{pc}	Fib (μm)
C15	1	—	—	—	—	—	—	—
C11	30	24.30	1.01	16.6	0	762	0.138	0
C14	30	31.07	1.29	45.7	955	—	—	0 to 45
C21	30	37.63	1.56	111.0	225	—	—	35 to 190
Average	30	31.00	1.29	57.7	393	762	0.138	—
C08	60	22.15	0.89	18.3	0	715	0.070	0
C13	60	18.62	0.75	7.9	0	673	0.040	0
C19	60	36.75	1.48	67.6	251	—	—	0 to 43
Average	60	25.84	1.04	31.3	83	694	0.055	—
C04	120	20.09	0.79	8.5	0	700	0.047	0
C16	120	32.93	1.29	16.5	0	—	—	0
C20	120	21.95	0.86	13.2	0	720	0.065	0
Average	120	24.99	0.98	12.7	0	710	0.056	0
C01	240	17.84	0.68	8.9	0	704	0.036	0
C05	240	23.52	0.90	12.4	0	742	0.075	0
C18	240	14.50	0.55	6.1	0	680	0.022	0
Average	240	18.62	0.71	9.1	0	708	0.044	0
C09	360	11.66	0.44	4.4	0	658	0.018	0
C12	360	16.17	0.60	10.2	0	683	0.030	0
C17	360	17.44	0.65	10.0	0	705	0.036	0
Average	360	15.09	0.56	8.2	0	682	0.028	0
C06	500	11.37	0.42	5.1	0	680	0.016	0
C07	500	16.17	0.59	8.5	0	705	0.033	0
C10	500	10.00	0.37	4.3	0	670	0.013	0
Average	500	12.51	0.46	6.0	0	685	0.021	0

Note: V = loading rate, P_f = fracture load, P_{gy} = general yield load, W = absorbed energy for fracture, X_f = distance from cleavage origin to notch tip, σ_f = local cleavage fracture stress, ε_{pc} = plastic strain at cleavage initiating position, and Fib = length of fibrous crack.

was observed, and further increasing the loading rate leads to a slight additional decrease in the notch toughness. For the FG microstructure, the effect of loading rate was not apparent and was obscured by the scatter of values measured at various loading rates. But, a slight decrease in toughness with increasing loading rate could still be seen. The notch toughness of the FG microstructure is appreciably larger than that of the CG one.

2. *Results of microscopic observation*

The parameters measured on the fracture surfaces are summarized in Tables II and III. The following ideas are summarized from experimental observations and the data of Tables II and III.

1. For the CG specimens in Table II: The fracture mode in the specimen with the lowest loading rate of 1 mm/min

Table III. The Parameters Measured from 4PB Tests for the Specimens with Various Loading Rates for FG

Number	V (mm/min)	P_f (kg)	P_f/P_{gy}	W (J)	X_f (μm)	σ_f (Mpa)	ε_{pc}	d_{fib} (μm)
X08	60	—	—	—	—	—	—	—
X07	120	43.12	1.60	68.3	521	1333	0.090	0
X11	120	52.33	1.94	103.7	261	—	—	47 to 170
X19	120	53.12	1.97	140.4	184	—	—	35 to 180
Average	120	49.52	1.84	104.1	322	1333	0.090	—
X03	240	48.22	1.72	81.9	300	1320	0.265	0
X13	240	47.53	1.69	72.4	447	1345	0.123	0
Average	240	47.88	1.71	77.1	373	1333	0.194	—
X02	360	35.77	1.24	47.5	718	1355	0.019	0
X10	360	49.78	1.73	90.1	535	—	—	30 to 180
X18	360	63.41	2.20	176.4	1033	1363	0.032	0
Average	360	49.65	1.72	104.8	762	1369	0.026	—
X01	500	40.47	1.38	59.9	150	1220	0.367	0
X05	500	45.47	1.54	84.4	327	—	—	30 to 170
X17	500	49.49	1.68	101.6	319	1330	0.253	0
Average	500	45.14	1.53	82.0	265	1275	0.310	—

The definitions are the same as in Table II.

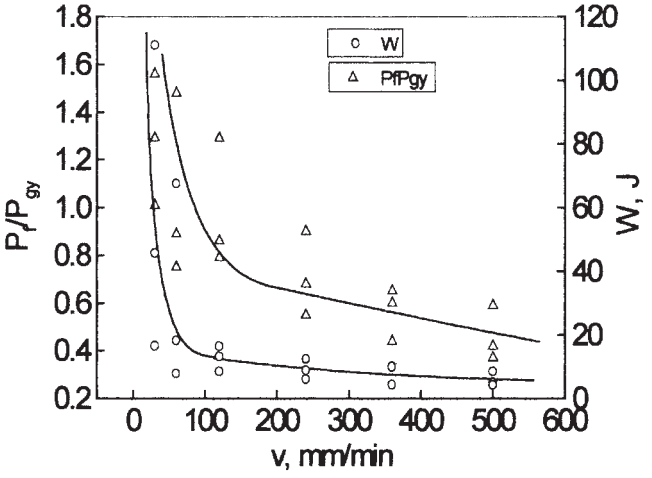

Fig. 11—The variations of notch toughness (characterized by the ratio of fracture load to general yield load, P_f/P_{gy}, and the absorbed energy for fracture, W) against the loading rate V for CG microstructure.

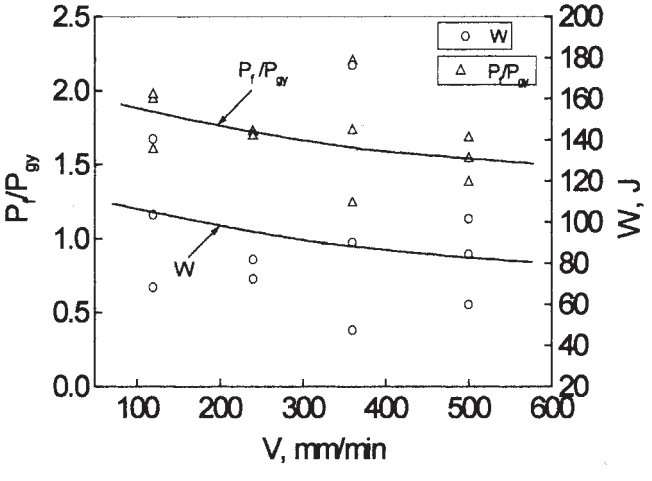

Fig. 12—The variations of notch toughness (characterized by the ratio of fracture load to general yield load, P_f/P_{gy}, and the absorbed energy for fracture, W) against the loading rate V for FG microstructure.

(No. C15) is ductile tearing without cleavage. In some specimens with lower loading rates of 30 and 60 mm/min (C14, C21, and C19), some short fibrous cracks (their average lengths, "Fib," are listed in Table II) emanating from the notch occur before cleavage initiation. Cleavage is initiated at a distance from the fibrous crack tip ahead of the notch root, as typically shown in Figure 13(a). In metallographic sections of fractured doubly notched specimens with lower loading rates of 30 and 60 mm/min, the remaining cracks located in the bright lamellar colony (pearlite colony–sized cracks, indicated by the black arrow 1 in Figure 14) and the remaining cracks located at gray matrix grains (ferrite grain–sized cracks, indicated by the white arrow 2 in Figure 14) were found in front of the surviving notch. This means that cleavage initiates in pearlite colonies or ferrite grains and that the critical crack size for cleavage propagation is the same size as the pearlite colony or ferrite grain.[18]

Most specimens with higher loading rates of 120 to 500 mm/min exhibit "zero values" of X_f (the distance from the cleavage-initiating site to the notch root is zero). In this case, cleavage is directly initiated at the notch tip, as shown in Figure 13(b). In metallographic sections of fractured doubly notched specimens with higher loading rates of 120 to 500 m/min, no remaining cracks were found.

2. For the FG specimens (in Table III): The fracture mode in the specimens with loading rates lower than 60 mm/min (such as X08) is ductile tearing without cleavage. These specimens have not been included in Table III. In some specimens with loading rates from 120 to 500 mm/min (X11, X19, X10, and X05), some short fibrous cracks (their average lengths are listed in Table III) emanating from the notch root also occur before cleavage initiation (Figure 15(a)). The cleavage of all specimens is initiated at nonzero distances (Table III) ahead of the notch root, as typically shown in Figure 15. In metallographic sections of fractured doubly notched specimens with these loading rates, the remaining cracks located in the bright lamellar colony (pearlite colony–sized cracks, indicated by the black arrow 1 in Figure 16) and the remaining cracks located in the gray matrix grains (ferrite grain–sized

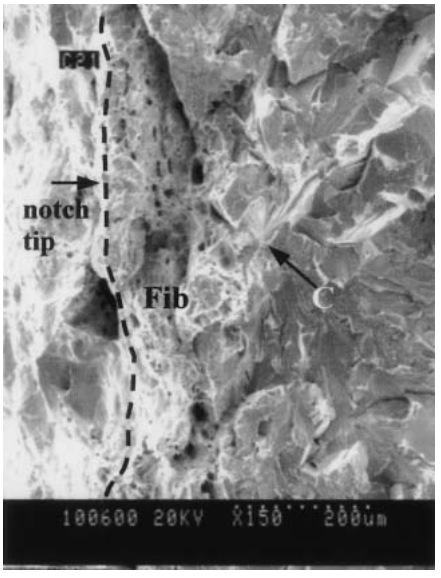

(*a*)

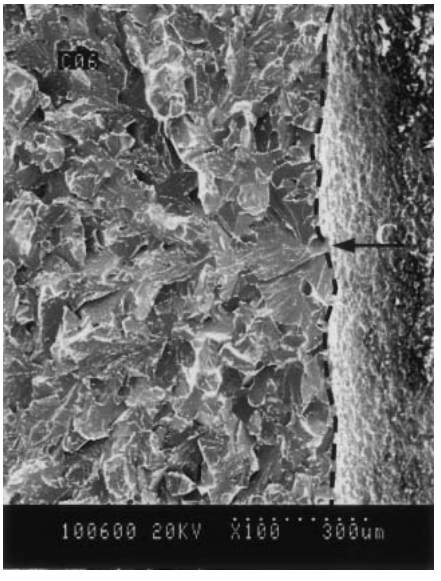

(*b*)

Fig. 13—Typical fracture surfaces showing cleavage initiation by a black arrow C for CG microstructure: (*a*) specimen (C21) with short fibrous crack at a loading rate of $V = 30$ mm/min; and (*b*) specimen (C06) without fibrous crack at a loading rate of $V = 500$ mm/min.

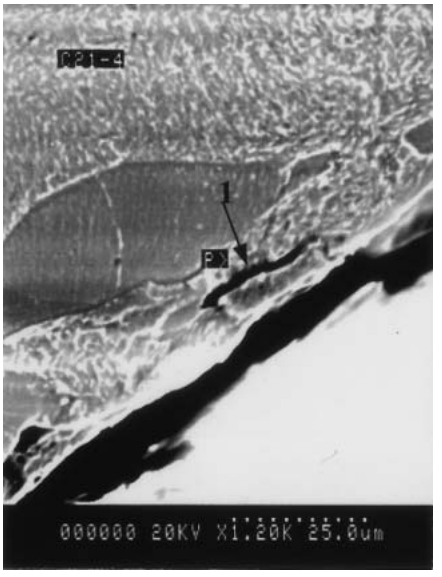

(*a*)

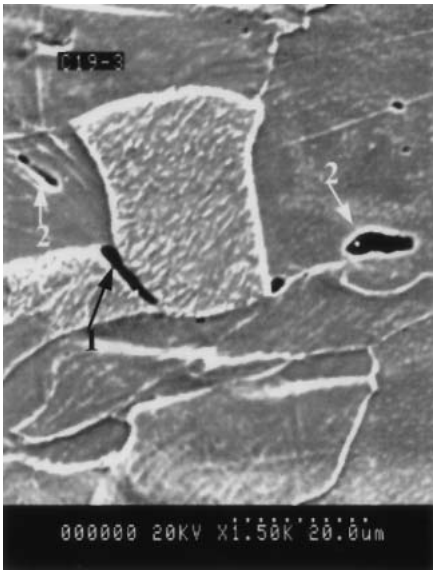

(*b*)

Fig. 14—Pearlite colony-sized (black arrow 1) and ferrite grain-sized (white arrow 2) remaining microscopic cracks found in front of the survived notch of the fractured doubly notched specimens for CG microstructure: (*a*) loading rate $V = 30$ mm/min; and (*b*) $V = 60$ mm/min.

cracks, indicated by the white arrow 2 in Figure 16) were also found in front of the surviving notch.

IV. DISCUSSION

A. *Effects of Loading Rate on the Critical Event for Cleavage*

A critical event, being the most important link in a process of cleavage, is defined as the most difficult step among the three consecutive steps of a cleavage process; *i.e.*, a crack nucleating in a second-phase particle, the just-nucleated crack passing through the boundary between the second-phase particle and the matrix grain, and the propagation of the grain-sized crack across the grain boundary. From the late 1960s to the 1980s, the critical event of cleavage was considered as the propagation of a second-phase particle-sized crack into the matrix.[19–22]

However, in recent years, some studies[10,11,23] found that while the normal tensile stress ahead of a notch root, exceeding the critical local fracture stress, is able to propagate a crack of critical size, the plastic strain may not have reached a critical value for nucleating a crack nucleus. It means that in some cases, the crack nucleation still behaves as a critical step for a cleavage process. Therefore, for producing

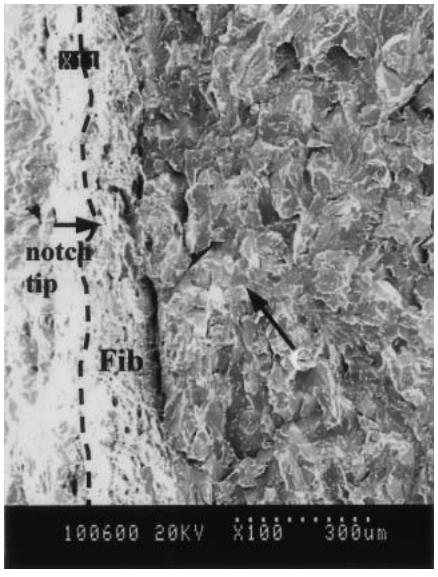

(*a*)

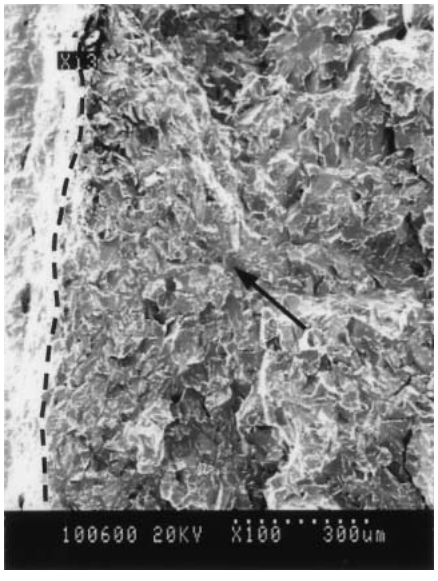

(*b*)

Fig. 15—Typical fracture surfaces showing cleavage initiation by a black arrow C for FG microstructure: (*a*) specimen (X11) with short fibrous crack at a loading rate of $V = 120$ mm/min; and (*b*) specimen (X13) without fibrous crack at a loading rate of $V = 240$ mm/min.

(*a*)

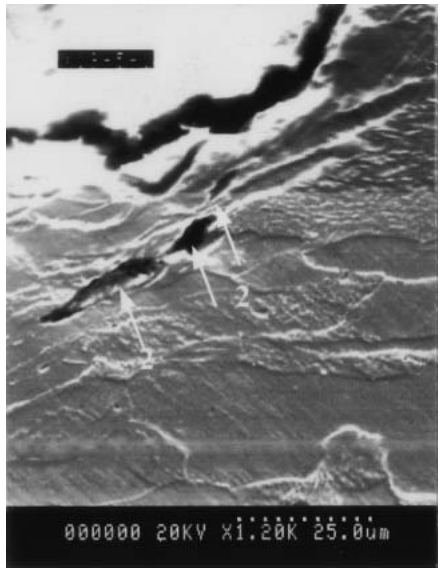

(*b*)

Fig. 16—Pearlite colony-sized (black arrow 1) and ferrite grain-sized (white arrow 2) remaining microscopic cracks found in front of the survived notch of the fractured doubly notched specimens for FG microstructure: (*a*) loading rate $V = 360$ mm/min; and (*b*) $V = 120$ mm/min.

cleavage, both criteria (a critical plastic strain ($\varepsilon_p \geq \varepsilon_{pc}$) to nucleate a crack and a critical normal stress ($\sigma_{yy} \geq \sigma_f$) to propagate the just-nucleated crack) should be reached. Thus, a dual criterion was suggested.[10,11,12]

On the other hand, some researchers[24,25,26] suggested that the critical event can be changed from the propagation of a grain-sized crack through the propagation of a second-phase particle-sized crack to the nucleation of a crack by increasing the acuity of a defect[24,25] or decreasing the temperature.[26] In recent works,[27,28] it has also been found that with increasing grain sizes and decreasing second-phase particles, the critical event can be changed from the propagation of a grain-sized crack to a crack-nucleation–dominated model,[27] and increasing the prestrain and decreasing the temperature facilitates the critical event changing from the propagation of a nucleated microcrack to the nucleation of the microcrack and then deteriorates the toughness.[28] However, the question of whether the critical events for cleavage could be changed by various loading rates has not yet been clarified.

The characteristic feature of a critical event of crack propagation controlled by tensile stress is that the cracks located in the microstructural domain that nucleated but failed to propagate remain in a fractured specimen. Doubly notched specimens are particularly appropriate for observing the remaining cracks in front of the surviving notch after the specimen is fractured at one notch. This is because when fracture occurred at one notch, the critical condition was

also reached in the vicinity of the surviving notch. That a crack remains in front of the surviving notch means that the tensile stress was not sufficient to propagate the crack just nucleated. This shows a tensile stress–controlling crack-propagation mechanism. When a large plastic strain is established ahead of a notch root, the cracks could be nucleated. But, if the tensile stress established ahead of the notch is insufficient to propagate a nucleated crack in a cleavage manner, a fibrous crack may be formed at the notch root due to the increasing large plastic strain with increasing applied load. With the extension of the fibrous crack, the tension stress ahead of its tip increases and makes a nucleated crack propagate, and the fibrous cracking changes to cleavage cracking.[29] Therefore, fibrous cracking occurring before cleavage initiation is also an indication of insufficient tensile stress to propagate a nucleated crack in a cleavage manner. This also shows a critical event of tensile stress–controlling crack propagation.[29] The phenomenon that cleavage initiates at nonzero distances ahead of the notch root, where the tensile stress is high, also supports the identification of the critical event of crack propagation.[27]

However, the characteristic feature of a critical event of crack nucleation is that no remaining crack can be found in fractured specimens. Another characteristic feature of the critical event of crack nucleation is that the site of cleavage initiation is located at the notch tip, where the plastic strain is very high. Because crack nucleation is plastic strain–controlled, the fact that cleavage fracture initiates at the notch tip implies that the local plastic strain for nucleating cracks plays an important role in the cleavage-fracture process, and the cleavage is nucleation controlled.[10,11,27,28]

1. *Critical event for cleavage of CG specimens*

In this work, it is found in Table II that among the three specimens with loading rates of 30 mm/min, short fibrous cracks occurred before cleavage in two specimens, and, in one doubly notched specimen, a pearlite colony–sized crack (as shown in Figure 14(a)) being very close to the surviving notch tip remains, indicating that the critical event is propagation of a pearlite colony–sized crack controlled by tensile stress. But in one specimen, the cleavage initiated at the notch tip and propagated directly at a lower applied load. These facts mean that the critical event of crack propagation dominates the cleavage-fracture process, but there is the possibility of nucleation-controlled fracture.

Among the three specimens with a loading rate of 60 mm/min, fibrous cracking was observed in one specimen, and pearlite colony–sized (indicated by the black arrow 1 in Figure 14(b)) and ferrite grain–sized (indicated by the white arrow 2 in Figure 14(b)) remaining microscopic cracks are also found in front of the surviving notch of the fractured doubly notched specimen. But, in the other two specimens, cleavage initiated at the notch tip and propagated directly, suggesting the critical event of crack nucleation. Therefore, mixed critical events of crack nucleation and crack propagation, under a critical mechanical condition, appear in this group with a greater tendency for a crack nucleation–controlled critical event.

In Table II, it can be further found that for the 12 specimens with loading rates larger than 120 mm/min, the cleavage initiates at the tip of the notch ($X_f = 0$), a site subjected to the highest plastic strain (Figure 9), which characterizes the nucleation-controlled critical event. The facts that no remaining cracks and no fibrous cracking were found in these specimens also support the nucleation-controlled critical event.

Therefore, it can be concluded that with increasing loading rates, the critical event of cleavage fracture can be changed from the propagation of a pearlite colony–sized crack or a ferrite grain–sized crack, through the mixed critical events of crack propagation and crack nucleation, to crack nucleation. The reason for the change of the critical event is analyzed as follows.

Recent works[10,11,12] suggested that the cleavage fracture in notched specimens must satisfy a dual criterion, *i.e.*, a critical plastic strain ($\varepsilon_p \geq \varepsilon_{pc}$) for initiating a crack nucleus, and a critical tensile stress ($\sigma_{yy} \geq \sigma_f$) for its propagation. Cleavage fracture initiates in an active zone determined by the dual criterion ahead of a notch root. From the FEM calculation obtained in this work, Figure 17(a) can be drawn, in which the stress at the notch tip (σ_{yyt}) and the peak stress (σ_{yymax})

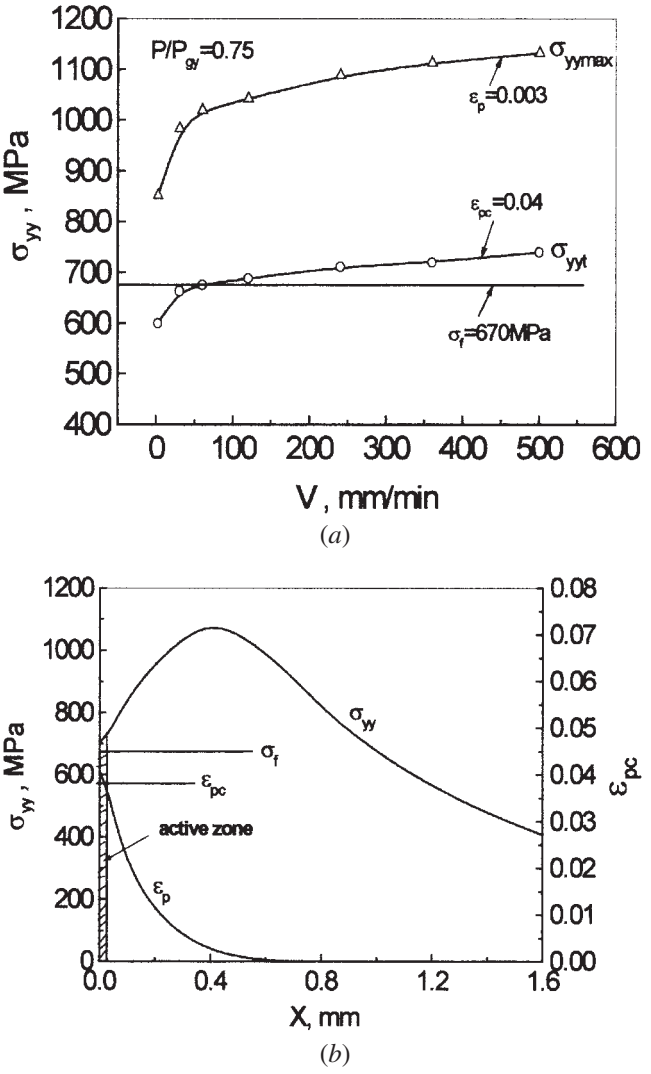

Fig. 17—The schematics for analyzing the critical events of cleavage fracture: (*a*) stress σ_{yyt} at the notch tip and the peak stress σ_{yymax} ahead of notch for various loading rates V for the CG specimens loaded to the same applied load ratio $P/P_{gy} = 0.75$; and (*b*) the stress and plastic strain distributions ahead of the notch tip for CG specimens loaded at 240 mm/min at average fracture load. The critical values of ε_{pc} and σ_f are also drawn.

ahead of the notch, for various loading rates for the CG specimens loaded to the same applied load ratio of $P/P_{gy} = 0.75$, are given. At this applied-load ratio, the plastic strain at the notch tip just reaches its average critical value of $\varepsilon_{pc} = 0.04$ (Table II) for initiating a crack nucleus, which represents the crack-nucleation strain of the most-weak constituents in the CG steel.[30] From Table II, the lower boundary value of σ_f is taken as the critical fracture stress,[28,30] and its value is about 670 MPa and is also drawn in Figure 17(a). From this figure, it could be found that when the loading rate is lower than 60 mm/min, while the plastic strain at the notch tip reaches the critical value of $\varepsilon_{pc} = 0.04$ and a crack could be nucleated, the tensile stress at the notch tip is lower than the critical value of $\sigma_f = 670$ MPa. Therefore, the crack cannot be propagated at the notch tip directly. Thus, in this case, cleavage is mainly controlled by crack propagation. While at this applied-load ratio the stress σ_{yy} around the location of the peak stress σ_{yymax} ahead of the notch exceeds the σ_f value for crack propagation, the plastic strain there is only about 0.003 and is insufficient to nucleate a crack. When the loading rate is around 60 mm/min, the dual criteria ($\varepsilon_p \geq \varepsilon_{pc}$ and $\sigma_{yy} \geq \sigma_f$) are both just satisfied near the notch tip, and the mixed critical events of the crack nucleation and crack propagation appear. When the loading rate is larger than 60 m/min, the stress at the notch tip exceeds σ_f. Once a crack nucleates at the notch tip, it will propagate and the X_f value will be zero (Table II). Thus, in this case, cleavage is controlled by crack nucleation. Figure 17(b) further shows this case. In Figure 17(b), the stress and plastic-strain distributions ahead of the notch tip for the CG specimens loaded at 240 mm/min at the average fracture load of the three specimens of $V = 240$ mm/min in Table II are given, and the critical values of ε_{pc} and σ_f are also drawn. From this Figure, it can be seen that the stress at the notch tip exceeds σ_f, but the cleavage only can occur in the small active zone (shaded area) at the notch tip, which is determined by the crack-nucleation criterion $\varepsilon_p \geq \varepsilon_{pc}$. This is the general case in specimens with loading rates larger than 60 mm/min in Table II.

From the previous analysis, it can be seen that for the CG microstructure with a lower σ_f value, the increase of the stress at the notch tip by increasing the loading rate facilitates the change of the critical event.

2. *Critical event for cleavage of FG specimens*

As described in the results from microscopic observation (Table III) Figures 15 and 16 show that remaining cracks and fibrous cracking were found, and the cleavage was initiated at nonzero distances ahead of the notch root for the FG specimens in the loading-rate range from 120 to 500 mm/min. According to the analysis of the characteristic feature of a critical event of crack propagation described previously, these facts mean that the critical event of the FG steel is crack propagation and does not change with increasing loading rate from 120 to 500 mm/min. The reason for this could be analyzed as follows.

Figure 18(a) gives the stress at the notch tip and the peak stress ahead of the notch for various loading rates for the FG specimens loaded to the same applied-load ratio ($P/P_{gy} = 0.97$), at which the plastic strain at the notch tip just reaches its average critical value of $\varepsilon_{pc} = 0.15$ (Table III) for initiating a crack nucleus; this represents the crack-nucleation strain of the weakest constituents in the FG steel.[30]

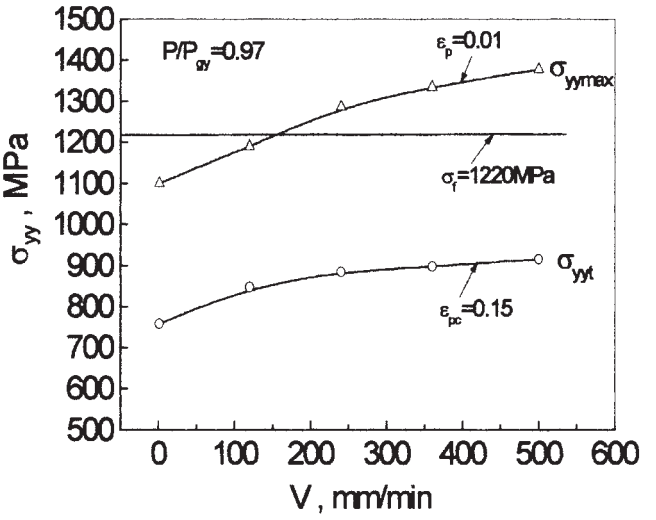

(*a*)

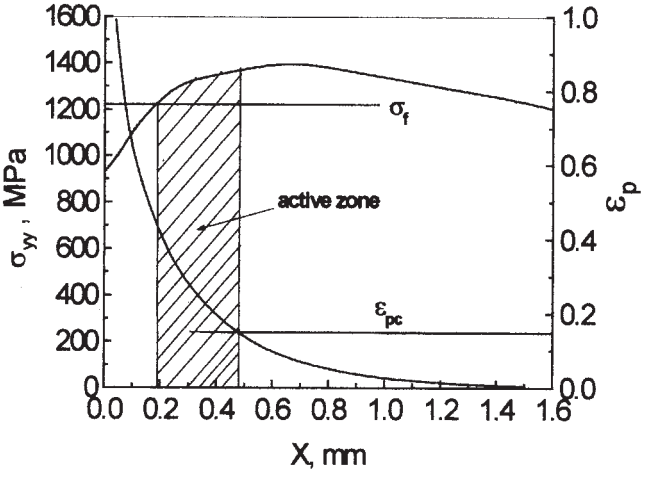

(*b*)

Fig. 18—The schematics for analyzing the critical events of cleavage fracture: (*a*) stress σ_{yyt} at the notch tip and the peak stress σ_{yymax} ahead of notch for various loading rates V for the FG specimens loaded to the same applied load ratio $P/P_{gy} = 0.97$; and (*b*) the stress and plastic strain distributions ahead of the notch tip for FG specimens loaded at 240 mm/min at average fracture load. The critical values of ε_{pc} and σ_f are also drawn.

From Table III, the lower boundary value of σ_f is taken as 1220 MPa and is drawn in Figure 18(a). From this figure, it could be found that in the loading-rate range tested from 1 to 500 mm/min, the stress at the notch tip is always much lower than σ_f, and the nucleated microcracks could not be propagated and then are blunted (Figure 16). For the specimens with loading rates lower than 60 mm/min, the criterion $\sigma_{yy} \geq \sigma_f$ for cleavage is never satisfied in front of notch; thus, the fracture mode in these specimens is the ductile tearing. For the specimens with loading rates larger than 120 mm/min, the peak stress ahead of the notch exceeds the σ_f value for crack propagation, but the plastic strain there is only about 0.01 and is insufficient to nucleate a crack. With further increasing applied load, the cleavage occurs due to the dual criteria ($\varepsilon_p \geq \varepsilon_{pc}$ and $\sigma_{yy} \geq \sigma_f$) satisfied at a site ($X_f$) from notch tip, or a fibrous crack may develop

at the notch tip due to the insufficient tensile stress for crack propagation in a cleavage manner before the dual criteria are satisfied. These processes combining the experimental results show a critical event of crack propagation, but there is also the possibility of nucleation-controlled fracture due to the first satisfaction of the condition $\sigma_{yy} \geq \sigma_f$ in the dual criteria for the weakest constituents with lowest the σ_f value in the steel.[30] Figure 18(b) further shows this case. In Figure 18(b), the stress and plastic-strain distributions ahead of the notch tip for the FG specimens loaded at 240 mm/min at the average fracture load of the three specimens of $V =$ 240 mm/min in Table III are given, and the critical values of ε_{pc} and σ_f are also drawn. From this figure, it could be seen that the stress at the notch tip is always lower σ_f, and the cleavage only can occur in the active zone (shaded area) away from the notch tip, which is mainly determined by the crack-propagation criterion $\sigma_{yy} \geq \sigma_f$. This is the general case for the specimens with loading rates larger than 120 mm/min in Table III.

From the previous analysis, it can be seen that for the FG microstructure, the unchanged critical event in the tested loading-rate range mainly arises from its higher cleavage-fracture stress.

B. *Effects of Loading Rate on the Local Cleavage-Fracture Stress*

The local cleavage-fracture stress is regarded as a decisive factor controlling the cleavage fracture and toughness of various steels.[26–38] A great number of works have found that σ_f is a very stable parameter and is an intrinsic property of steel.[35–38] The σ_f value is determined as the value of the tensile stress σ_{yyc} at the cleavage-initiation site X_f, which is measured at the fracture load. It is considered to be nearly independent of test temperature[17,25,31,35] and specimen geometry.[37,38]

However, the effects of loading rate on σ_f have not been completely validated. In previous works,[25,35] σ_f values estimated from Charpy V-impact tests are essentially the same as those measured by 4PB specimens tested at quasi-static loading; thus, it is considered that σ_f is nearly independent of loading rate. In this work, the σ_f values are accurately measured by 4PB tests combining the FEM calculation of stress distribution ahead of the notch at various loading rates.

Figure 19 shows the local cleavage-fracture stress of the CG specimens with the critical event of crack nucleation and of the FG specimens with the critical event of crack propagation at various loading rates. It could be found that with increasing loading rate, σ_f remains nearly a constant of about 700 and 1325 MPa for the CG and FG microstructures, respectively, with a scatter band of $\pm$50 MPa. The σ_f value is mainly determined by the critical event of the cleavage fracture.[18,21] The discussion in Section IV–A has shown that in the loading-rate range tested, the critical event of the CG specimens is mainly the crack nucleation, and that of the FG specimens is mainly crack propagation. While the loading rate varies, the critical event of the CG and FG specimens in Figure 19 does not change, and, therefore, the cleavage micromechanism does not change in the different specimens. This can be considered as the microscopic reason for the independence of σ_f on loading rate.

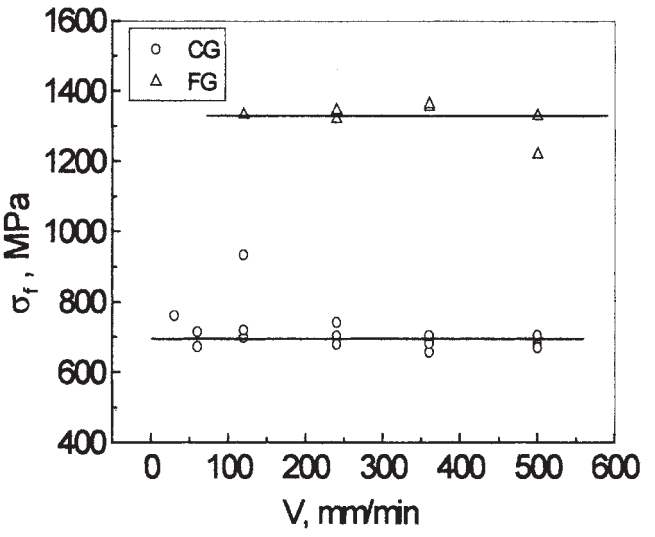

Fig. 19—The local cleavage fracture stress σ_f of the CG and FG specimens loaded at various loading rates.

On the other hand, Figure 19 also shows that the σ_f value of the FG microstructure is higher than that of the CG one. From Figures 2 and 3, the sizes of the coarsest ferrite grains and pearlite colonies in the CG microstructure are around 160 and 140 μm, and these of the FG microstructure are around 65 and 60 μm, respectively. This difference causes the difference in σ_f.[27,35,39,40] The size distribution of ferrite grains and pearlite colonies causes the scatter of the measured σ_f values.[35]

C. *Effects of Loading Rate on Notch Toughness*

From Figure 11, for the CG microstructure, an appreciable drop in notch toughness of specimens with a loading rate of around 60 mm/min was observed, and further increasing the loading rate leads to a slight additional decrease in notch toughness. For the FG microstructure (Figure 12), the effect of loading rate was not apparent, and only a slight decrease in toughness with increasing loading rate could be seen. This behavior in toughness is consistent with the variation of the critical event for cleavage. For the CG specimens tested at 60 mm/min, a 70 MPa increase in yield strength causes the same increase in the stress at the notch tip. Because σ_f is low (670 MPa), the increase of yield strength causes the change of the critical event from the mixed critical events of crack nucleation and crack propagation to crack nucleation, and the fracture load decreases. A further increase in σ_y by increasing the loading rate to 500 mm/min does not affect the critical event; thus, the change of the toughness is small. The slight decrease in toughness with increasing loading rates larger than 120 mm/min is caused by the slight decrease of ε_{pc} (Table II).[27] For FG specimens tested at loading rates from 120 to 500 mm/min, the critical event is crack propagation and does not change with loading rate; thus, the toughness also does not change significantly. The slight decrease in toughness with increasing loading rate is caused by the increase of the stress ahead of the notch by increasing the loading rate (Figures 10(a) and 18(a)).

From Figures 11 and 12, it also could be found that the notch toughness of the FG microstructure is appreciably higher than that of the CG one, and the fracture behavior of the FG microstructure is not sensitive to loading rate. The local fracture stress is a key parameter determining the notch toughness.[27] Steel with a fine grain size and high σ_f value presents a critical event of a grain-size–controlled crack propagation and a high toughness. Increasing ε_{pc} can further improve the toughness. Therefore, the high notch toughness of the FG microstructure arises from its high σ_f and ε_{pc} values. The phenomenon that fracture behavior of the FG microstructure is not sensitive to loading rate is caused by the unchanging critical event with increasing loading rate. Therefore, it could be suggested that the FG steel could be used in the engineering structures with higher loading rates. On the other hand, the low toughness of the CG microstructure mainly results from its low σ_f value.

V. SUMMARY

From this work of four-point bending tests of notched specimens loaded at various loading rates for a low-alloy steel with different grain sizes, combining the microscopic observation and FEM calculations, the following conclusions can be drawn.

1. With increasing loading rate, the general yield load and the peak stress ahead of notches increase, but the location of peak stress does not change significantly.
2. For the CG microstructure, an appreciable drop in notch toughness with a loading rate of around 60 mm/min was observed, and further increasing the loading rate leads to a slight additional decrease in notch toughness. For the FG microstructure, the effect of loading rate was not apparent. The change in toughness of the CG microstructure resulted from a change of the critical event controlling the cleavage fracture with increasing loading rate.
3. For the CG microstructure with a lower cleavage-fracture stress, with increasing loading rates, the critical event of cleavage fracture can be changed from the propagation of a pearlite colony–sized crack or a ferrite grain–sized crack, through the mixed critical events of crack propagation and crack nucleation, then to crack nucleation. This change deteriorates the toughness. The increase of the stress at the notch tip by increasing the loading rate facilitates the change of critical event.
4. For the FG microstructure with a higher cleavage-fracture stress, the critical event of cleavage fracture is the crack propagation in the loading-rate range from 120 to 500 mm/min. The unchanging critical event mainly arises from the higher cleavage-fracture stress of this microstructure.
5. With increasing loading rate, the cleavage-fracture stress remains nearly a constant of about 700 and 1325 MPa for the CG and FG microstructures, respectively, with a scatter band of ± 50 MPa. The reason for this is that the critical event of cleavage fracture does not change in the specimens for measuring σ_f. The higher cleavage-fracture stress of the FG microstructure is caused by its finer grain size. The higher notch toughness of the FG microstructure is caused by its finer grain size. The higher notch toughness of the FG microstructure arises from its higher σ_f value and the critical plastic strain for initiating a crack nucleus, and the fracture behavior of this FG steel is not sensitive to loading rate in the range of this work.

ACKNOWLEDGMENT

This work was financially supported by the Key Research and Development Program for Outstanding Group and the State Key Laboratory of Nonferrous Metal Materials at the Lanzhou University of Technology (Gansu University of Technology).

REFERENCES

1. D.A. Curry, I. Milne, and R.S. Gates: *Mater. Sci. Eng*., 1984, vol. 63, pp. 101-09.
2. H. Couque, R.J. Asaro, J. Duffy, and S.H. Lee: *Metall Trans. A*, 1988, vol. 19A, pp. 2179-206.
3. A.K. Zurek, P.S. Follansbee, and J. Hack: *Metall. Trans. A*, 1990, vol. 21A, pp. 431-39.
4. S. Lee, J.W. Rhyu, K.M. Cho, and J. Duffy: *Metall. Trans. A*, 1993, vol. 24A, pp. 901-12.
5. H. Qiu, H. Mori, M. Enoki, and T. Kishi: *Metall. Mater. Trans. A*, 2000, vol. 31A, pp. 2785-91.
6. A. Venkert, P.R. Gudure, and G. Ravichandran: *J. Eng. Mater. Technol*., 2001, vol. 123, pp. 261-67.
7. M.S. Mirza, D.C. Barton, and P. Church: *J. Mater. Sci*., 1996, vol. 31, pp. 453-61.
8. J.H. Yoon, B.S. Lee, Y.J. Oh, and J.H. Hong: *Int. J. Pressure Vessels Piping*, 1999, vol. 76, pp. 663-70.
9. V. Jablokov, D.M. Goto, D.A. Koss, and J.B. McKirgan: *Mater. Sci. Eng. A*, 2001, vol. 302, pp. 197-205.
10. M.G. Mendiratta, R.L. Goetz, and D.M. Dimiduk: *Metall. Mater. Trans. A*, 1996, vol. 27A, pp. 3903-12.
11. G.Z. Wang and J.H. Chen: *Int. J. Fract*., 1998, vol. 89, pp. 269-84.
12. J.J. Lewandowski and A.W. Thompson: *Acta Metall*. 1987, vol. 35, pp. 1453-66.
13. J.H. Chen and C. Yan: *Mater. Sci. Technol*., 1988, vol. 4, pp. 732-39.
14. D.J. Alexander, J.J. Lewandowski, W.J. Sisak, and A.W. Thompson: *J. Mech. Phys. Solids*, 1986, vol. 34, pp. 433-54.
15. M. Srinivas and S.V. Kamat: *Mater. Sci. Technol*., 2001, vol. 17, pp. 529-35.
16. J.S. Lin: Ph.D. Thesis, Xian Jiaotong University, Xian, China, 1989.
17. J.R. Griffiths and D.R.J. Owen: *J. Mech. Phys. Solids*, 1971, vol. 19, pp. 419-31.
18. J.H. Chen, G.Z. Wang, Y. Chen, H. Ma, and L. Zhu: *Int. J. Fract*., 1997, vol. 83, pp. 105-20.
19. C.J. McMahon and M. Cohen: *Acta Metall*., 1965, vol. 13, pp. 591-605.
20. E. Smith: *Proc. Conf. on the Physical Basis of Yield and Fracture*, Physics Society, Oxford, United Kingdom, 1966, pp. 36-53.
21. D.A. Curry and J.F. Knott: *Mater. Sci*., 1978, Nov., pp. 511-14.
22. G.T. Hahn: *Metall. Trans. A*, 1984, vol. 15A, pp. 947-59.
23. M. Wall, C.E. Lane, and C.A. Hippsley: *Acta Metall. Mater*., 1994, vol. 42, pp. 1295-309.
24. G. Oates and J.R. Griffiths: *Met. Sci. J*., 1869, vol. 3, pp. 111-15.
25. J.H. Chen., G.Z. Wang, and H. Ma: *Metall. Trans. A*, 1990, vol. 21A, pp. 321-30.
26. T. Lin, A.G. Evans, and R.O. Ritchie: *J. Mech. Phys. Solids*, 1986, vol. 34, pp. 477-97.
27. J.H. Chen, G.Z. Wang, and Q. Wang: *Metall. Mater. Trans. A*, 2002, vol. 33A, pp. 3393-402.
28. J.H. Chen, Z. Li, and G.Z. Wang: *Metall. Mater. Trans. A*, 2003, vol. 34A, pp. 1055-68.
29. G.Z. Wang, J.H. Chen, and Z.H. Li: *Metall. Mater. Trans. A*, 1997, vol. 28A, pp. 1689-99.
30. G.Z. Wang and J.H. Chen: *Fatigue Fract. Eng. Mater. Struct*., 2001, vol. 24, pp. 451-59.
31. R.O. Ritchie, J.F. Knott, and J.R. Rice: *J. Mech. Phys. Solids*, 1973, vol. 21, pp. 395-410.
32. F.M. Beremin: *Metall. Trans. A*, 1983, vol. 14A, pp. 2277-87.

33. J.J. Lewandowski and A.W. Thompson: *Metall. Trans. A*, 1986, vol. 17A, pp. 1769-86.
34. A.V. Samant and J.J. Lewandowski: *Metall. Mater. Trans. A*, 1997, vol. 28A, pp. 389-99.
35. J.H. Chen, L. Zhu, and H. Ma: *Acta Metall. Mater.*, 1990, vol. 38, pp. 2527-35.
36. J.H. Chen, X.J. Hu, and G.Z. Wang: *Fatigue Fract. Eng. Mater. Struct.*, 1996, vol. 19, pp. 68-80.
37. G.Z. Wang, H.J. Wang, and J.H. Chen: *Fatigue Fract. Eng. Mater. Struct.*, 1999, vol. 22, pp. 849-58.
38. G.Z. Wang, G.H. Liu, and J.H. Chen: *Int. J. Fract.*, 2001, vol. 112, pp. 183-96
39. D.A. Curry: *Met. Sci.*, 1980, vol. 14, pp. 319-23.
40. T. Miyata, R.C. Yang, A. Otsuka, T. Haze, and S. Ahira: *Advances in Fracture Research*, Proc. ICF6, K Salama, K. Ravi-Chander, R. Taplin, and P. Rama Rao, eds., Pergamon Press, Houston, TX, 1989, pp. 2563-572.